atmosphere

MDPI

Article

Optimization of Discharging Electrodes of a Multi-Chamber Electrostatic Precipitator for Small Heat Sources

Michal Holubčík [1,*], Juraj Drga [1], Nikola Čajová Kantová [2], Jan Najser [3] and Jaroslav Frantík [3]

[1] Department of Power Engineering, Faculty of Mechanical Engineering, University of Žilina, Univerzitna 1, 010 26 Žilina, Slovakia
[2] Research Centre, University of Žilina, Univerzitna 1, 010 26 Žilina, Slovakia
[3] Centre of Energy Utilization of Non-traditional Energy Sources—ENET Centre, VSB—Technical University of Ostrava, 17. listopadu 2172/15, 708 00 Ostrava, Czech Republic
* Correspondence: michal.holubcik@fstroj.uniza.sk

Abstract: On the way to reducing emissions released into the atmosphere, there is an obstacle in the form of the emissions of solid pollutants produced by households, namely the burning of solid fuels in small heat sources. In this article, the authors deal with the development of a low-cost electrostatic precipitator, which would be able to significantly reduce the production of particulate matter. This is a tubular precipitator concept, which is enhanced by dividing the precipitation space into four chambers, each of which has an ionization electrode. With the investigated structural arrangement, it is possible to increase the size of the collection area without affecting the external dimensions of the separator. The essence of this article was to focus on the design of an ionization electrode, which, in addition to the function of a negative electrode, would also fulfill the function of a structural element of the proposed geometry. The work contains a technical design for the shape of the ionization electrode, which was subsequently examined using ANSYS Fluent software. The conditions under which a corona discharge will occur on the electrodes and how particulate matter is captured in the separation device were investigated with the help of simulations of the electric field intensity. According to the achieved simulation results, calculations were made for the theoretical efficiency of particle collection, which reached a value of approximately 78%.

Keywords: particulate matter; electrostatic precipitator; reducing emissions; corona discharge

Citation: Holubčík, M.; Drga, J.; Čajová Kantová, N.; Najser, J.; Frantík, J. Optimization of Discharging Electrodes of a Multi-Chamber Electrostatic Precipitator for Small Heat Sources. *Atmosphere* **2023**, *14*, 63. https://doi.org/10.3390/atmos14010063

Academic Editor: Honglei Wang

Received: 28 November 2022
Revised: 16 December 2022
Accepted: 26 December 2022
Published: 29 December 2022

1. Introduction

Recently, the trend of "green" energy, reducing consumption and thus reducing harmful impacts on nature [1] has been promoted worldwide. Humanity is moving toward the elimination of combustion engines in transport, the use of public transport services, and the construction of low-energy dwellings. This effort should lead to sustainability and protection not only for the atmosphere but for the entire spectrum of the environment [2,3]. A significant factor that directly affects the level of air pollution is particulate matter (PM) emissions. These emissions damage human health and can cause serious respiratory and cardiovascular diseases and even brain-cell disorders [4–6]. Their source can be fuel from combustion processes, agricultural and industrial activity, energy, or soil erosion. It is also necessary to mention road traffic as a source of PM when solid particles are released into the air due to the movement of vehicles on asphalt roads [7,8]. Every year, the European Union publishes an annual report for emissions production in all sectors and proposes appropriate measures to reduce environmental pollution. The state of the air report for 2022 indicates that the reduction in PM emissions is moving in a positive direction, except for countries such as Poland, Kosovo, Italy, Bosnia and Herzegovina, Serbia, and North Macedonia, which lag significantly behind others in the concentration of PM in the atmosphere. [9]. The Slovak Republic sits just below the upper limit of emission limits.

This work focused on the release of PM into the atmosphere produced by the combustion of solid fuel in small heat sources. It is therefore an area of heating in households, for which the EU has not yet introduced emission limits and measures as it has. However, it can be assumed that in the coming years, attention will be focused on household heating. This is also indicated by the results of air monitoring by the Slovak Hydrometeorological Institute in the territory of the Slovak Republic for the year 2022, where the share of PM10 and PM2.5 emissions in the household heating sector shows the highest values. The production of PM10 emissions from households represents 14.397 kt (60.1%) of total PM10 production, and PM2.5 production from households represents 14.067 kt (80.5%) of total PM2.5 production [10].

Reducing PM production from small heat sources is possible in several ways. The primary way is based on ensuring the most efficient solid fuel combustion process [11,12]. The second way is where attention is now focused, i.e., capturing PM in the chimney, outside the combustion space. The electrostatic precipitation of particles appears to be a suitable choice for the secondary reduction in PM emissions, due to its potential to achieve a capture efficiency above 90%.

A lot of work has been devoted to this topic for a long time and several commercially available separation devices have been created. However, these devices were not a commercial success due to their high price and low availability in Slovak market conditions. Our attention is therefore directed toward the development of ESP, which is financially undemanding for the consumer and can ensure a significant reduction in PM emissions being emitted into the atmosphere. The principle of operation of ESP is not inherently complex but consists of relatively complicated processes that take place during precipitation. The main condition is the achievement of a corona discharge on the charging electrode, which occurs when the value of the initial critical voltage supplied to the electrode is exceeded. When investigating the formation of a corona discharge, the use of CFD simulations is a suitable tool, which can facilitate complicated calculations of the corona discharge itself, the influence of the location and distance of the charging electrodes, etc. Tarasov et al. performed a simulation of a DC electric discharge, obtaining three-dimensional distributions of temperature and current density during the discharge [13]. Dhayef et al., in their research, devoted themselves to the simulation of corona discharges in the pipeline of an ESP with a charging electrode radius of 0.5 mm and an electrode distance of 50 mm. The supplied voltage was set at 20 kV and the flow velocity, pressure, and temperature were set at 1 m/s, 1 atm, and 293.15 K. From the results, they concluded that the shape of the electrodes and the operating parameters of the ESP had a significant impact on the investment and operating costs of the device, as well as on the efficiency of PM capture [14]. Kawamoto conducted an interesting study looking at the ESP of dust particles in the atmosphere of Mars, comparing these conditions to those on Earth. The capture efficiency on Mars was generated at around 75%, while Earth conditions showed an efficiency of around 95%. The main difference in the input parameters was the low atmospheric pressure of Mars. This also affected the more significant deposition of dust on the surfaces of the charging electrodes, which the author reduced by mechanically cleaning the electrodes using vibrations [15]. Skodras et al. created a CFD model of an ESP where, using 2D geometry, they monitored the behavior of gas flow through the precipitator, particle trajectories, and electrostatic parameters of the device. The settings of the performed simulations and the achieved values of the monitored quantities are completely described in the work [16]. Dong et al. investigated the influence of the applied voltage and the distance between the electrodes on the separation process using simulations. They concluded that increasing the voltage within the allowed range had a positive effect on the capture efficiency. On the other hand, they found that the particles that were injected in the center of the channel were affected the most intensively; on the contrary, the particles injected approximately 5 mm from the center of the channel were the least affected. The authors also compared three placements for the electrodes, and the third version of the geometric arrangement appeared to be the most effective [17]. Dong et al. later also investigated the use of a charging electrode that contained spikes. They found that the vortices that form near the tip of the electrode improve the efficiency of particle collection. They also investigated the effect of the location of the tips upstream and downstream of the gas flow [18]. Zukeran et al. focused on the study of charge and particle trajectory in the ESP with parallel plates as collection electrodes and the effect of the number of charging electrodes on the separation process. With the help of experimental measurement using the PIV method, they confirmed the simulated processes, which coincided to a sufficient extent. They proved that an ESP arrangement with three charging electrodes shows better results than the application of only one electrode [19]. Zhao et al. performed a similar plate ESP experiment where they focused on the particle collection efficiency achieved under different external operating conditions. The achieved PM10 and PM2.5 capture efficiencies ranged from 86.9% to 99% [20]. Becker et al. built a needle into the charging electrode to charge the particles in the ESP. They simulated the electrostatic field, the ion space charge field, and the field around the needle. The results compared with the experimentally determined V/A characteristics showed a satisfactory correlation and served for further research on the given topic [21]. Everson et al. performed a computational model verification of a multi-electrode parallel ESP with tip elements on the electrodes. They observed the obtained results of operating parameters such as plate distance, inter-electrode distance, number and shape of electrodes, applied voltage, particle size, and gas flow [22]. Yook et al. focused on a different shape of charging electrodes with tips. They investigated different electrode geometries, while numerical calculations were verified experimentally. The collection efficiency of the ESP increased by about 15% with the optimized discharge electrode, and the power consumption and ozone generation showed little difference after optimization [23].

2. Materials and Methods

2.1. Concept of an Investigated Electrostatic Precipitator

This article is focused on the concept of a tubular ESP. A cross-section of a classic steel chimney pipe, considered the collecting electrode, was divided into four chambers using a partition made of two aluminum sheets welded in the shape of a cross, as shown in Figure 1. There is a charging electrode in each of the chambers which means that the number of charging electrodes has increased compared to the classic tubular separator. Due to the partitioning of the separating chamber, the collection area of the ESP has also been significantly increased. At the same time, the structural arrangement of the division of the chambers does not significantly reduce the cross-section of the ESP, so the gas flow velocity does not increase significantly either. M4 threaded rods were designed as collector electrodes to ensure the structural strength of the assembly, which represents their important advantage. Their disadvantage, resulting from the given concept of the ESP, is that it is necessary to supply a voltage higher than 35 kV for a corona discharge to occur. Therefore, a solution was devised which optimized the threaded rods using spike elements so that the corona discharge occurs more readily at a voltage of 20 kV and, at the same time, the electrodes represented a structural connecting element. This is the main essence of this publication, and it includes numerical calculations of the operating parameters of the ESP, CFD simulations of the generated electric field, and drawing documentation for the proposed charging electrodes and the entire device. Later, laboratory measurements of the device's efficiency will be performed based on the designs that are investigated in this work.

Due to the modification of the geometry, it was possible to increase the collection area of the ESP more than twice without affecting the external dimensions of the device. A comparison of the sizes of the collection surfaces of a simple tubular ESP and the ESP with four chambers is shown in Table 1.

The entire geometry of the ESP is shown in Figure 2. The length of the ESP was set at 1 m with a diameter of 300 mm. At the inlet of the ESP, there is an expansion from a 200 mm pipe to a 300 mm one, or 300/200 at the outlet due to the easier connection of the ESP to the chimney available in the laboratory. The four charging electrodes were formed from M4 threaded rods and connected at the top and bottom ends. Since they are a connecting material, the whole structure is held together by threaded rods. The set of charging electrodes is separated from the collection electrodes (partition and external chimney pipe Ø 300 mm) by ceramic inserts to achieve the necessary insulation.

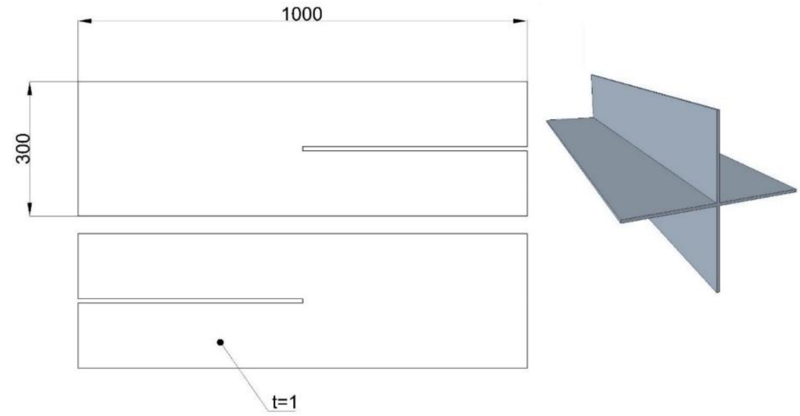

Figure 1. Partition made of two sheets, welded in the shape of a cross.

Table 1. Increase in the collection area.

Length of Precipitator 1 m	Collecting Area [m^2]
Tubular precipitator with one ionization electrode and one collecting electrode Ø = 300 mm	0.94
Tubular precipitator with four ionization electrodes and one collecting electrode Ø = 300 mm with cross-shaped partition	2.14

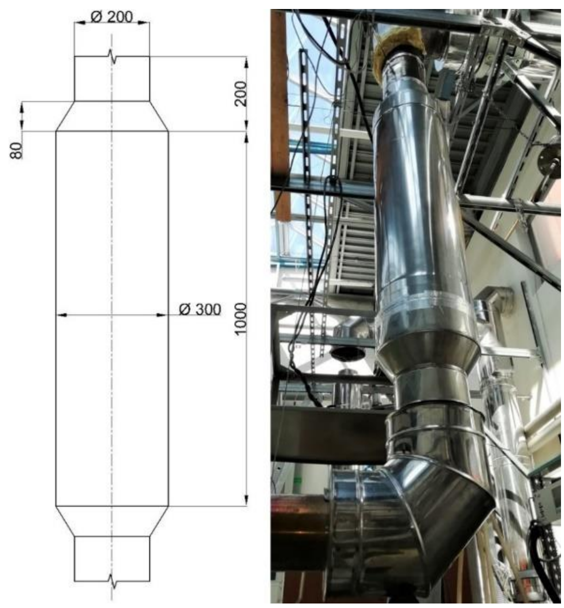

Figure 2. The geometry of the precipitator.

The CX-600A transformer was used as the DC voltage source 5–60 kV, with an output current of 3–5 mA, as shown in Figure 3. These parameters meet the needs of our equipment and at the same time, it is a power source with low investment costs.

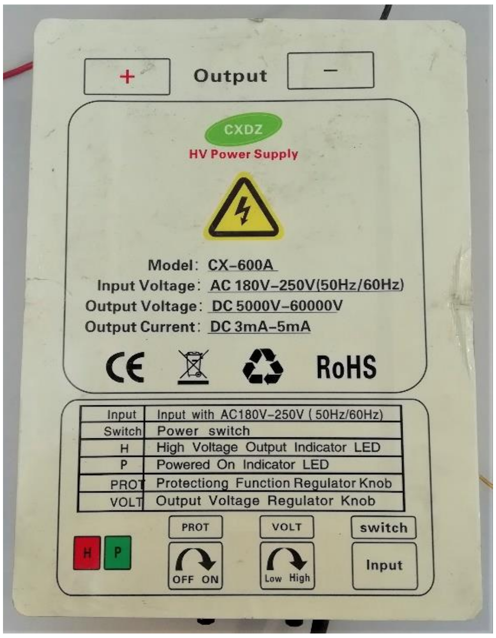

Figure 3. DC power supply.

2.2. Boundary Conditions of the Model

Due to their thickness, the threaded rods themselves made it possible to create a corona discharge at higher voltages, which would also cause high energy consumption. For this reason, it was decided to adjust the shape of the threaded rods using spike elements. Due to such treatment, edges with a small diameter were formed on the surface of the electrodes, on which the corona discharge was achieved at a much lower applied voltage. Calculations were made to determine the value of the initial critical field strength for a threaded rod electrode without spikes. This value served rather as a reference value when evaluating the results of numerical simulations for the electrodes with tips. The calculations were based on equations from the available literature as the calculations of the initial critical electric field intensity, the initial critical voltage, and the radius of the ionization region [24].

The critical initial field strength was calculated according to Equation (1):

$$E_{0c} = k_1 \vartheta \left[1 + \frac{k_2}{\sqrt{(\vartheta r)}} \right] \left[\mathrm{V{\cdot}m^{-1}} \right] \tag{1}$$

where k_1 and k_2 are quantities of the Whitehead–Brown equation, ϑ is the relative gas density and r is the radius of the discharge electrode.

The critical initial voltage was calculated according to Equation (2):

$$U_{0c} = r\, E_{0c} \ln\left(\frac{R}{r}\right) [\mathrm{V}] \tag{2}$$

where R is the radius of the collecting electrode.

The radius of the ionization region as a pure gas was calculated according to Equation (3):

$$z = \frac{1}{2\vartheta} \left[\frac{2U}{k_1 ln\left(\frac{R}{r}\right)} + k_2^2 - k_2 \sqrt{\left(\frac{4U}{k_1 ln\left(\frac{R}{r}\right)} + k_2^2 \right)} \right] [\mathrm{m}] \tag{3}$$

where U is the applied voltage.

The radius of the collecting electrode was adjusted according to the solved geometry. Since the cross-section of the ESP was divided, it was necessary to perform calculations with a collection electrode diameter of less than 300 mm. The new diameter of the electrode for calculations was set at 124 mm, as explained in Figure 4.

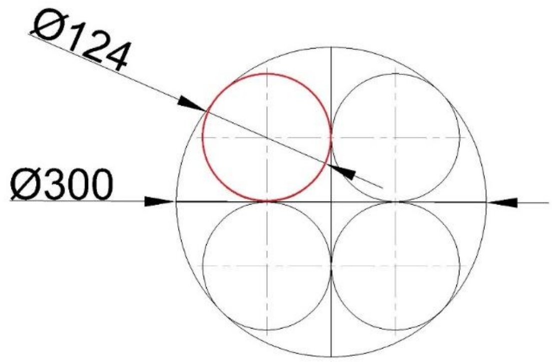

Figure 4. Diameter of one chamber modified for calculations.

2.3. Numerical Simulations

The previous calculations could not be applied to the modified shape of the tipped electrode. Therefore, it was necessary to carry out a numerical simulation that would describe in more detail the effect of changing the shape of the electrode on its electrical parameters. A suitable tool for more complex calculations is ANSYS Fluent, which is also used in the development of other devices that reduce the impact of emissions on the atmosphere [25].

The spike elements were created from sheet metal cutouts which are fixed on the threaded rod from both sides using threaded nuts. Such a construction allows for flexibility in setting the distance of individual spikes, and at the same time, it represents a low investment cost. The geometry of the electrode tips is shown in Figure 5.

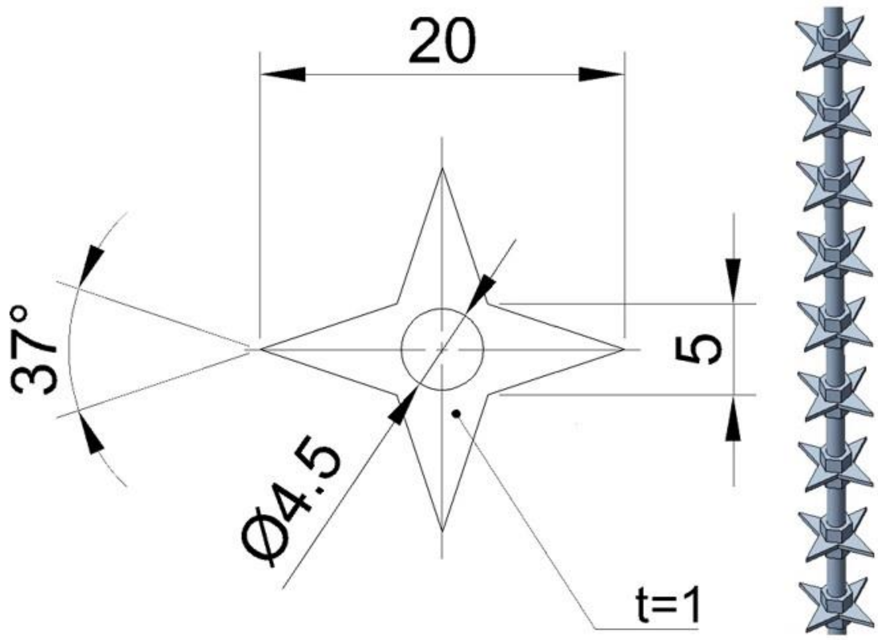

Figure 5. Spike elements for discharging electrode.

Based on the modified geometry of the charging electrodes, numerical simulations of the generated electric field were performed. Calculations were performed with ANSYS Fluent software using the MHD module for electric potential. Since it was an investigation of the intensity of the electrode, a simplified 3D geometry consisting of an M4 rod and one tip element was used. They were placed in a cylindrical space with a diameter of 124 mm. For completeness, the simulation of the electric field for the electrode without a tip was also performed. The simplified geometry for the numerical simulation is shown in Figure 6.

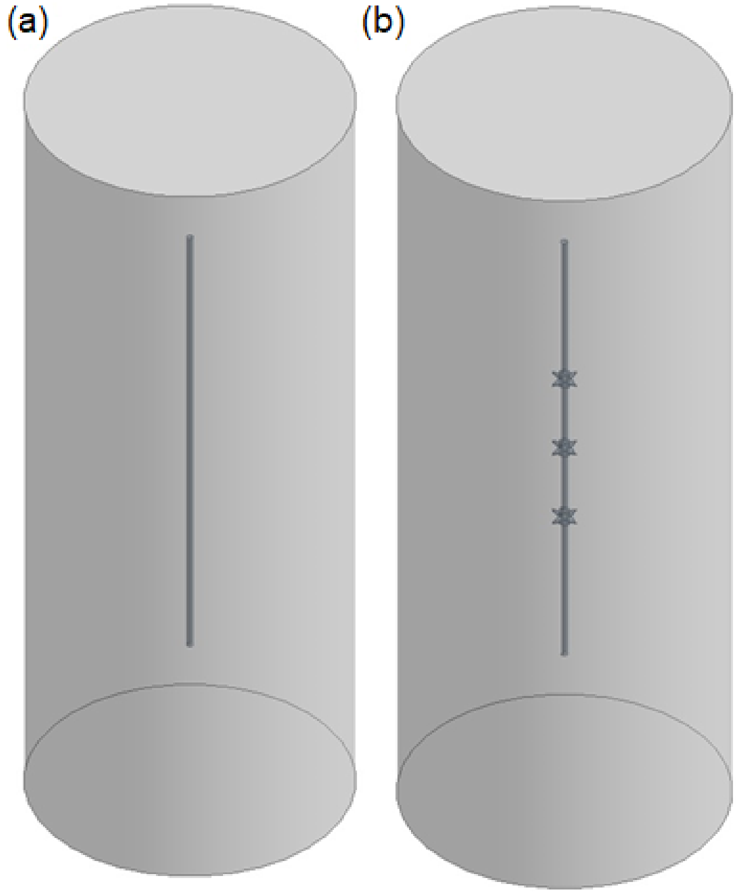

Figure 6. Simplified geometry used for simulations (**a**) without spike elements and (**b**) with spike elements.

The mesh of the model with the spike-shaped electrode consisted of 1,678,121 tetrahedral cells. The quality of the mesh was considered very good based on an average value of the orthogonal quality at 0.77, and the skewness at 0.23. The mesh of the model without spiked elements electrode consisted of 1,431,263 tetrahedral cells. The quality of the mesh was considered very good based on an average value of the orthogonal quality at 0.78, and the skewness at 0.22. The simulation was based on the k-omega SST turbulence model with an MHD module for simulating the electrical field. The electrical potential was set up for 20 kV on the discharging electrode and 0 V for the collecting electrode. In terms of boundary conditions, an inlet velocity of 0.5 m/s was applied at the inlet. Turbulence was defined as 5% for turbulent backflow intensity and 10 for turbulent backflow turbulent viscosity ratio for both inlet and outlet. The boundaries of the precipitators were defined as stationary walls with no-slip shear conditions. The simulation was performed for one chamber. The intensity of the electric field near the collecting electrode is much lower than near the ionization electrode, which also results from the principle of the device's function. Therefore, in the work, we assumed that the electric fields of the individual chambers would not influence each other through the metal partition.

2.4. Numerical Calculations of Precipitator Theoretical Efficiency

Based on the proposed parameters and the achieved results, it was possible to determine the theoretical efficiency of particle separation in the device. Calculations of the separation efficiency for individual particle sizes were performed first (1 µm, 2.5 µm, 5 µm, and 10 µm) at the electric field intensity interval E (5.3–9.6 × 10^6 V·m^{-1}) for the gas flow velocity of 1–1.5 m·s^{-1}. According to Equation (4), the charge acquired by the particle when charged was calculated as follows [26]:

$$q = \pi d_p^2 \varepsilon_0 \frac{3\varepsilon}{2+\varepsilon} E_{ch} [\mathrm{C}] \tag{4}$$

where ε_0 is the permittivity of a vacuum (8.85 × 10^{-12} C·V^{-1}·m^{-1}), ε is the dielectric constant for the particle relative to the vacuum, E_{ch} is the charging field strength (V·m^{-1}), and d_p is the particle diameter.

Subsequently, it was possible to calculate the drift velocity according to Equation (5):

$$w = \frac{C_c q E}{3\pi\mu d_p} \left[\mathrm{m \cdot s^{-1}}\right] \tag{5}$$

where E is the electrical potential (V), C_c is the Cunningham slip factor depending on particle diameter, and μ is the fluid viscosity for air at 277 °C to simulate the temperature in the chimney.

The theoretical capture efficiency was calculated according to Equation (6):

$$\eta = 1 - \left(-\frac{wA}{Q}\right)[-] \tag{6}$$

where A is the collecting area (m^2) and Q is the gas flow (m^3·s^{-1}).

Based on these calculations, the overall theoretical efficiency of PM capture was carried out. The percentage distribution of particle size in the considered gas was defined based on the results of previous experimental measurements of PM in the gas [27]. The theoretical efficiency was considered according to Equation (7):

$$\eta = 0.38\eta_{\mathrm{PM1}} + 0.35\eta_{\mathrm{PM2.5}} + 0.22\eta_{\mathrm{PM5}} + 0.05\eta_{\mathrm{PM10}}\ [-] \tag{7}$$

where particle sizes of 1 µm, 2.5 µm, 5 µm, and 10 µm were considered.

3. Results

Figure 7 shows the construction of the electrostatic precipitator in reality, after applying the spike elements.

Figure 7. Construction of a device with spike elements.

Based on the defined relationships, the initial parameters of the tipless electrode were calculated, which served as reference values for the simulation results. The calculated values of the initial critical intensity of the electric field, the initial critical voltage, and the radius of the ionization zone are shown in Table 2.

Table 2. The initial critical intensity of the electric field, the initial critical voltage, and the radius of the ionization zone.

Quantity	Value
E0c	5.23×106 V·m^{-1}
U0c	3.59×104 V
z (at a supply voltage of 20 kV)	0.94 mm

From the results, it can be observed that corona discharge will not occur at the given supplied voltage. For it to occur, it is necessary to ensure that the value of the initial critical intensity of the electric field on the tip electrode exceeds 5.23×10^6 V·m^{-1}.

After performing a numerical simulation of the tip electrode, it was apparent that a sufficient electric field intensity would be generated in the vicinity of the tips to cause a corona discharge. The highest intensity was achieved in the area of sharp points of the spikes, up to 9.6×10^6 V·m^{-1}. Under such conditions, it is obvious that a corona discharge will occur. The size of the ionization zone of the precipitator will then depend on the number of spikes applied to the threaded rod. The distribution of the electric field intensity is shown in Figure 8.

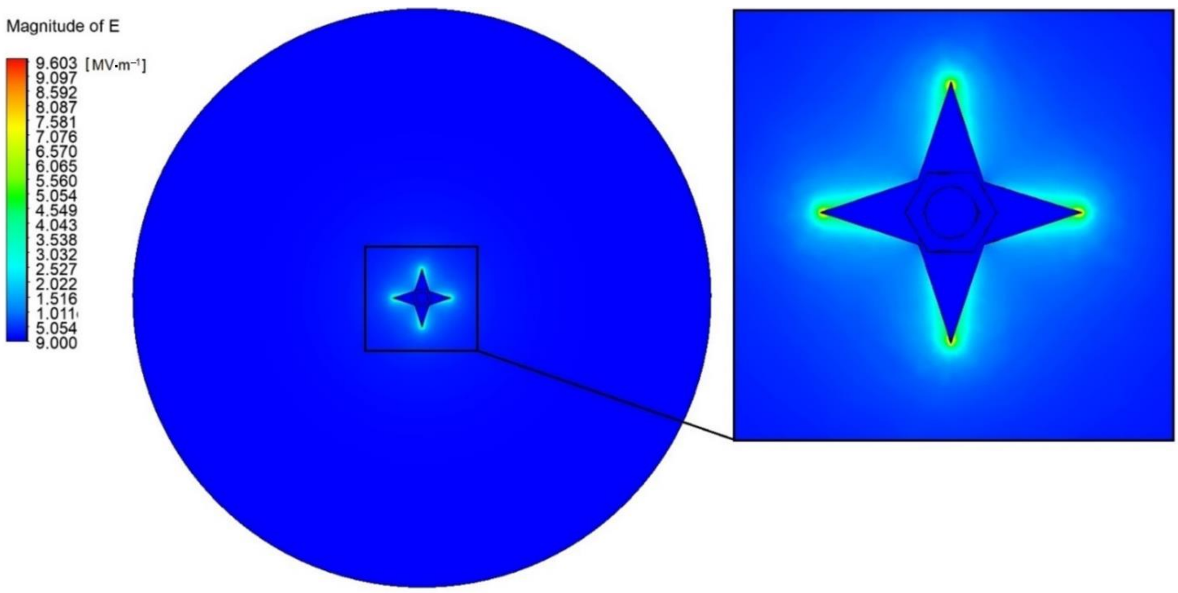

Figure 8. Range of electric field intensity on the electrode with spikes by numerical simulation.

Figure 9 shows the distribution of the electric field intensity on the electrode without tip elements. The result confirms the previous calculations. At a voltage of 20 kV, there will be no corona discharge on the surface of the electrode, because the electric field intensity will not exceed the calculated value of the initial critical field intensity. The achieved value of the electric field intensity was 3.09×10^6 V·m^{-1}.

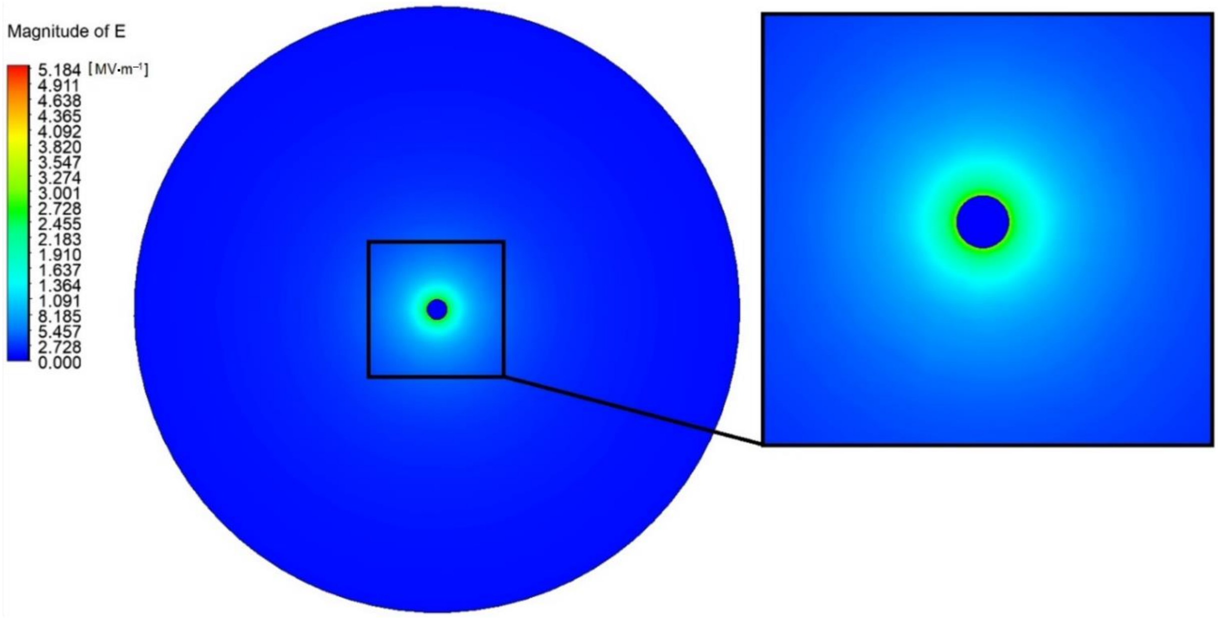

Figure 9. Range of electric field intensity on the electrode without spikes by numerical simulation.

According to the previously described equations, the values of particle capture efficiency were calculated depending on particle size, the strength of the electric field, and the gas flow rate. These dependencies are shown graphically in Figure 10. It is obvious that the highest efficiency will be achieved with particles with a larger diameter (PM5 and PM10).

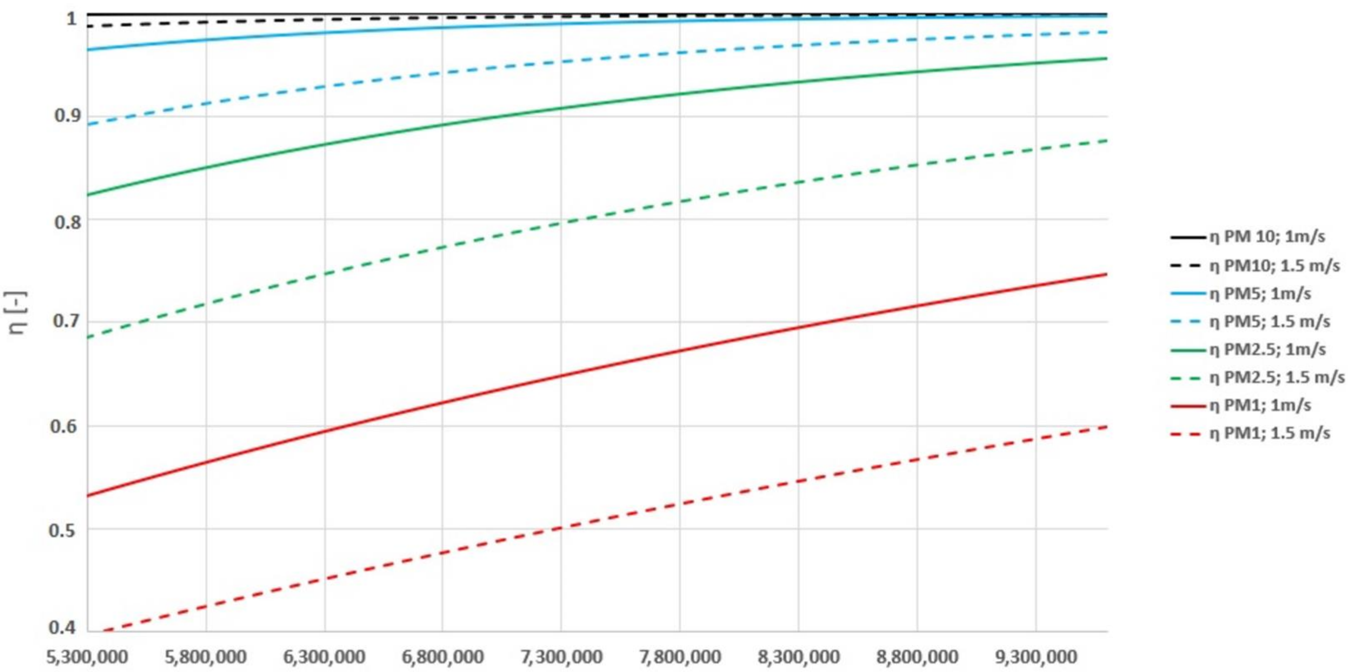

Figure 10. Collecting efficiency for different sizes of particles, depending on electrical field strength and gas velocity.

According to Equation (7), the theoretical particle capture efficiency was calculated for the whole range of PM sizes. The mean theoretical efficiency value reached 77.98%. The resulting efficiency for the range of gas speeds (1–1.5 $m \cdot s^{-1}$) and intensity of the electrical field (5.3–9.6 $\times 10^6$ $V \cdot m^{-1}$) is shown graphically in Figure 11.

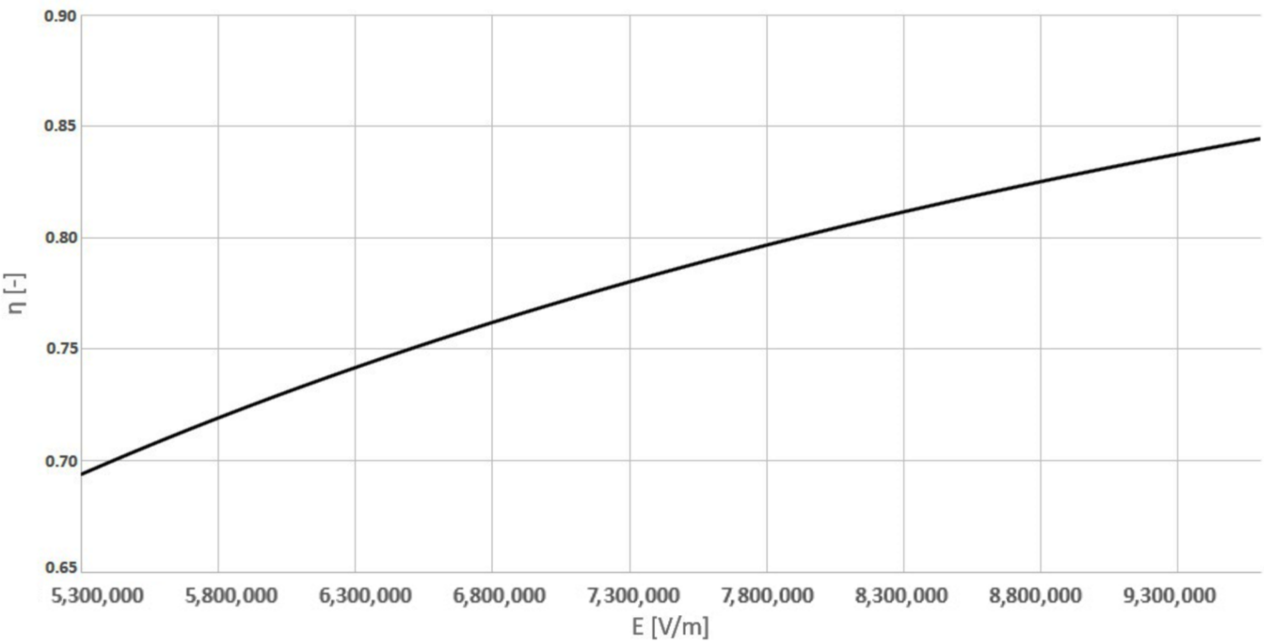

Figure 11. Theoretical efficiency of capture for the precipitator.

4. Conclusions

A significant element of atmospheric pollution in the long term is the production of PM from small heat sources, i.e., household heating. This is a sector in which measures to reduce PM production have not yet been implemented. Therefore, it is necessary to look for available solutions that would at least reduce the negative effects of this problem.

Electrostatic precipitators, which have been used in industry and the energy sector for a long time, offer a promising option. However, the commercial use of ESP in society has not yet found its application. The ESP for small heat sources differs from industrial heat sources in the geometric arrangement of the electrodes and the precipitation space. These are devices with a circular cross-section, most often located in a chimney pipe.

This work focused on modifying the geometry of a simple tubular ESP by a sheet metal partition in the shape of a cross. This modification makes it possible to divide the precipitation space into four equal chambers to increase the collection area of the ESP without changing the external dimensions of the device. M4 threaded rods were used as charge electrodes for their advantage in being used to connect the elements of the ESP so that there are no spatial deviations during operation. However, the threaded rods themselves require a high DC voltage supply above 36 kV to generate a corona discharge from their surface due to their large thickness. This is a necessary condition for the correct function of the ESP. It was therefore decided to modify the shape of the electrode to enable a corona discharge to occur more readily at a voltage of 20 kV. This results in lower power consumption from the voltage source. The modification was carried out using spiked elements fixed on the threaded rod. First, numerical calculations were performed to determine the critical initial electric field intensity, the critical initial voltage, and the radius of the ionization region for a threaded rod electrode without spikes. The critical intensity value was calculated to be 5.23×10^6 V·m^{-1}, which corresponded to a supply voltage of approximately 36 kV. These values served as reference values for subsequent numerical simulations of the generated electric field for the spiked electrodes. The results of the simulations for the spiked electrodes showed that it is possible to achieve an electric field intensity of up to 9.6×10^6 V·m^{-1}. This means that a corona discharge will occur at an applied voltage of 20 kV. For completeness, a simulation of the electric field around an electrode without spikes was also carried out, which confirmed the initial calculations. The value of the maximum field strength reached 3.09×10^6 V·m^{-1}, which guarantees only the creation of an electrostatic field without corona discharge. Subsequently, calculations of the theoretical efficiency of PM collection for the given precipitator were carried out. The results showed that with such a design solution, it is possible to achieve a device efficiency of 77.98%.

The accuracy of the calculations was influenced in the work by simplifying the cross-section of the chamber from a quarter circle to a circle, which results in a difference in the mutual distance between the ionization and collection electrodes of approximately 15%. The second factor, which has a greater influence on specific efficiency results, was the distribution of the concentration of particles in the flowing gas which affected the efficiency of capturing particles according to their size and also, therefore, the overall theoretical efficiency. The concentration distribution parameters were determined as average values based on previous measurements of PM in the flue gas in the chimney pipe without ESP installed; the difference in particle concentrations according to size between individual measurements was approximately 5–10%.

According to the obtained calculations, it was possible to assume a high efficiency in PM10 and PM2.5 particle capture, even in comparison with other works. With PM1, the calculated collection efficiency is lower compared to previous works, but it is also necessary to consider different operating parameters resulting from specific design solutions of the devices. Dong et al. in their simulation of the spiked electrode, at an applied voltage of 19.2–27.5 kV and a gas velocity of 1–1.3 $m \cdot s^{-1}$, achieved the collection efficiency of particles with a size of 0.2–1 μm in the range of 21–37% [18]. An interesting comparison results from the work of Caroll et al., in which three commercially available separators were compared when burning different types of wood. For PM1, Al-Top new achieved the highest efficiency of up to 92.6% when burning willow. OekoTube showed the lowest efficiency for PM1 when burning tall fescue, 35.7% [28]. Gao et al. achieved a capture efficiency of 94–97% for PM1 using their ESP prototype with a supply voltage of 22.3 kV. However, it is necessary to note that these values were achieved at a gas velocity of 0.24–0.36 $m \cdot s^{-1}$ [29]. If a lower gas flow velocity were considered in this work, the efficiency of PM1 would also increase, but it is clear from the measurements made so far that the gas velocity is approximately 1–1.5 $m \cdot s^{-1}$.

The achieved theoretical results of this work as the concept of the ESP will subsequently be investigated by laboratory measurements; the efficiency of PM collection will be measured as well as the effect of density, or distances of individual electrode spikes on the precipitation process itself.

Author Contributions: M.H., methodology, writing—review and editing, funding acquisition, supervision; J.D., methodology, writing—original draft preparation, data curation; N.Č.K., conceptualization and investigation; J.N., formal analysis; J.F., resources and validation. All authors have read and agreed to the published version of the manuscript.

Funding: This publication has been produced with the support of Slovak Research and Development Agency by project APVV-21-0452—Impact of using small electrostatic precipitators to reduce particulate pollutants in domestic fuel combustion, and Cultural and educational grant agency of the Ministry of Education, Science, Research and Sports of the Slovak Republic by project KEGA 032ŽU-4/2022—Implementation of knowledge about modern ways of reducing environmental burden in the energy use of solid fuels and waste into the pedagogical process.

Data Availability Statement: Data are available in a publicly accessible repository.

Conflicts of Interest: The funders had no role in the design of the study; in the collection, analyses, or interpretation of data; in the writing of the manuscript; or in the decision to publish the results. The authors declare no conflict of interest.

References

1. Floros, F. Green Energy in Europe and SocioEconomic Impact. *J. Manag. Strategy* **2022**, *13*, 31. [CrossRef]
2. Pezzuto, I. An Analysis of the Recent Eurozone Recovery: Is It Sustainable? *J. Gov. Regul.* **2017**, *6*, 2017. [CrossRef]
3. Taušová, M.; Tauš, P.; Domaracká, L. Sustainable Development According to Resource Productivity in the EU Environmental Policy Context. *Energies* **2022**, *15*, 4291. [CrossRef]

4. Jianhui, J.; Haddad, I.E.; Prévôt, A.S.H. Sources of particulate-matter air pollution and its oxidative potential in Europe. *Nature* **2020**, *587*, 414–419. [CrossRef]
5. Peters, R.; Ee, N.; Peters, J.; Anstey, K.J. Air Pollution and Dementia: A Systematic Review. *J. Alzheimer ´s Dis.* **2019**, *70*, 1–19. [CrossRef]
6. Pryor, J.T.; Cowley, L.O.; Simonds, S.E. The Physiological Effects of Air Pollution: Particulate Matter, Physiology and Disease. *Front. Public Health* **2022**, *10*, 882569. [CrossRef] [PubMed]
7. Kovalová, D.F.; Ďurčanská, D.; Hegrová, J. Impact of Asphalt Mixture Composition on Particulate Matter Production. *Procedia Eng.* **2017**, *192*, 201–206. [CrossRef]
8. Pospisil, J.; Huzlik, J.; Licbinsky, R.; Spilacek, M. Dispersion characteristics of PM10 particles identified by numerical simulation in the vicinity of roads passing through various types of urban areas. *Atmosphere* **2020**, *11*, 454. [CrossRef]
9. Europe's Air Quality Status 2022, Briefing no. 04/2022. Available online: https://www.eea.europa.eu/publications/status-of-air-quality-in-Europe-2022 (accessed on 25 November 2022).
10. Slovak Hydrometeorological Institute, Department of Emissions and Biofuels. 2022. Available online: https://www.enviroportal.sk/indicator/detail?id=141 (accessed on 25 November 2022).
11. Chabadova, J.; Papucik, S.; Nosek, R. Particle Emissions from Biomass Combustion. *AIP Conf. Proc.* **2014**, *1608*, 67–70. [CrossRef]
12. Klement, I.; Vilkovská, T.; Uhrín, M.; Baranski, J.; Konopka, A. Impact of high temperature drying process on beech wood containing tension wood. *Open Eng.* **2019**, *9*, 428–433. [CrossRef]
13. Tarasov, D.A.; Firsov, A.A. CFD simulation of DC-discharge in airflow. *J. Phys. Conf. Ser.* **2021**, *2100*, 012015. [CrossRef]
14. Dhayef, H.K.; Khalaf, T. Simulation of a Corona Discharge in a Wire-Duct Electrostatic Precipitator. *Project: Plasma Phys.* **2022**, *21*, 4603–4614.
15. Kawamoto, H.; Kobayakawa, T.; Ogino, Y.; Takabori, K. Electrostatic Precipitator in Martian Environment. *Proc. Space Eng. Conf.* **2018**, *28*, 1B2. [CrossRef]
16. Skodras, G.; Kaldis, S.P.; Sofialidis, D. Particulate removal via electrostatic precipitators—CFD simulation. *Fuel Process. Technol.* **2006**, *87*, 623–631. [CrossRef]
17. Dong, M.; Zhou, F.; Zhang, Y.; Li, S. Numerical study on fine-particle charging and transport behaviour in electrostatic precipitators. *Powder Technol.* **2018**, *330*, 210–218. [CrossRef]
18. Dong, M.; Zhou, F.; Zhang, Y.; Shang, Y.; Li, S. Numerical study on electrohydrodynamic flow and fine-particle collection efficiency in a spike electrode-plate electrostatic precipitator. *Powder Technol.* **2019**, *351*, 71–83. [CrossRef]
19. Tamura, R.; Ito, K.; Date, Y.; Taoka, T. Simulation and Measurement of Particle Trajectory in an Electrostatic Precipitator with Multiple Wire Electrodes. *IEEE Trans. Ind. Appl.* **2022**, *58*, 2452–2461. [CrossRef]
20. Knight, R.; Zhao, L.W.; Zhu, H. Modelling and optimization of a wire-plate ESP for mitigation of poultry PM emission using COMSOL. *Biosyst. Eng.* **2021**, *211*, 35–49. [CrossRef]
21. Beckers, S.C.; Pawlik, J.; Eren, H.; Kiel, J. Simulation of a Discharge Electrode Needle for Particle Charging in an Electrostatic Precipitator. *SNE Simul. Notes Eur.* **2021**, *31*, 233–238. [CrossRef]
22. Arif, S.; Branken, D.J.; Everson, R.C.; Arif, A. An experimentally validated computational model to predict the performance of a single-channel laboratory-scale electrostatic precipitator equipped with spiked and wire discharge electrodes. *J. Electrost.* **2021**, *112*, 103595. [CrossRef]
23. Lee, G.H.; Hwang, S.Y.; Cheon, T.W.; Yook, S.J. Optimization of pipe-and-spike discharge electrode shape for improving electrostatic precipitator collection efficiency. *Powder Technol.* **2020**, *379*, 241–250. [CrossRef]
24. Böhm, J. *Elektrické Odlučovače*; Müszaki Könyvkiadó (MLR), SNTL–Nakladatelství technické literatury (Č SSR), Verlag Technik (NDR): Praha, Czech Republic, 1977; 327p.
25. Rimar, M.; Fedak, M.; Kulikov, A.; Kulikova, O.; Lopusniak, M. Analysis and CFD Modeling of Thermal Collectors with a Tracker System. *Energies* **2022**, *15*, 6586. [CrossRef]
26. Kılıç, M.; Mutlu, M.; Altun, A.F. Numerical Simulation and Analytical Evaluation of the Collection Efficiency of the Particles in a Gas by the Wire-Plate Electrostatic Precipitators. *Appl. Sci.* **2022**, *12*, 6401. [CrossRef]
27. Holubčík, M.; Jandačka, J.; Ďurčanský, P.; Čaja, A. Particulate matter measurement by using the particle sizers APS and SMPS. *EAI Endorsed Trans. Energy Web.* **2020**, *8*, 166000. [CrossRef]
28. Carroll, J.; Finnan, J. Use of electrostatic precipitators in small-scale biomass furnaces to reduce particulate emissions from a range of feedstocks. *Biosyst. Eng.* **2017**, *163*, 94–102. [CrossRef]
29. Gao, X.; Zhang, Y.; Guo, Y.; Shen, Z.; Yang, Z.; Liu, S.; Liang, C.H.; Zheng, C.H. Balance and stability between particle collection and re-entrainment in a wide temperature-range electrostatic precipitator. *Powder Technol.* **2018**, *340*, 543–552. [CrossRef]